ESAIM: M2AN 49 (2015) 577–599
DOI: 10.1051/m2an/2014047

ESAIM: Mathematical Modelling and Numerical Analysis
www.esaim-m2an.org

RESIDUAL *A POSTERIORI* ERROR ESTIMATION FOR THE VIRTUAL ELEMENT METHOD FOR ELLIPTIC PROBLEMS

L. Beirão da Veiga[1] and G. Manzini[2,3]

Abstract. *A posteriori* error estimation and adaptivity are very useful in the context of the virtual element and mimetic discretization methods due to the flexibility of the meshes to which these numerical schemes can be applied. Nevertheless, developing error estimators for virtual and mimetic methods is not a straightforward task due to the lack of knowledge of the basis functions. In the new virtual element setting, we develop a residual based *a posteriori* error estimator for the Poisson problem with (piecewise) constant coefficients, that is proven to be reliable and efficient. We moreover show the numerical performance of the proposed estimator when it is combined with an adaptive strategy for the mesh refinement.

Mathematics Subject Classification. 65N30.

Received November 3, 2013. Revised June 30, 2014.
Published online 17 March 2015.

1. Introduction

The Virtual Element Method (VEM) is a very recent generalization of the Finite Element (FE) method [21,24] that achieves a higher degree of flexibility in terms of meshes and properties of the scheme by avoiding an explicit construction of the discrete shape functions. VEM was first introduced for the Poisson problem in [11] and, then, further developed in the papers [1,9,12,19]. The method has clearly a connection with classical polygonal and polyhedral finite elements, see for instance [15,16,29,33–37,40,41].

On the other hand, VEM makes use of a virtual discrete space and an approximated bilinear form $\mathcal{A}_h$ that mimics the original bilinear form withouth the need to integrate complex non-polynomial functions (and still guaranteeing consistency and stability of the numerical problem). The latter is a remarkable difference with respect to classical polyhedral/polygonal FEM. The Virtual Element Method has also a relation with the Mimetic Finite Difference (MFD) schemes, for a very short list see for instance [6,18,20,23,26,28] and the book [13] with the references therein.

Due to the large flexibility of the meshes to which the mimetic, polygonal and virtual methods are applied, mesh adaptivity becomes an appealing feature as mesh refinement and de-refinement strategies can be

Keywords and phrases. A posteriori error estimation, virtual element method, polygonal mesh, high-order scheme.

[1] Dipartimento di Matematica "F. Enriques", Università degli Studi di Milano, via Saldini 50, 20133 Milano, Italy. lourenco.beirao@unimi.it

[2] Applied Mathematics and Plasma Physics Group, Theoretical Division, Los Alamos National Laboratory, Los Alamos, NM 87545, USA. gmanzini@lanl.gov

[3] IMATI del CNR, via Ferrata 1, 27100 Pavia, Italy.

implemented very efficiently. Hanging nodes can be introduced in the mesh without spreading the refined zones in order to guarantee the mesh conformity. Polygonal cells with very general shapes are admissible thus allowing us to adopt simple mesh coarsening algorithms.

There is a vast literature about *a posteriori* error estimations for finite elements, see for instance the books [2,30,31,38] and the fundamental papers [4, 5]. Unfortunately, for the virtual element method the a posteriori error analysis is more involved as there is no explicit knowledge of the basis functions inside the elements and to devise residual-based error estimators (which are among the most popular ones in finite element analysis) is particularly difficult. The same difficulty is encountered in the MFD method; this is reflected by the fact that also in the mimetic literature (that is older than VEM) there are very few papers devoted to the a-posteriori analysis. In references [6, 8], the authors circumvent the absence of the shape functions by introducing a post-processed pressure solution that is used in the computation of the residual. This approach is successful for the MFD method [20] for the diffusion problem in mixed form. Regarding the diffusion problem in primal form, a hierarchical estimator has been recently proposed [3], which does not require any evaluation of residuals. This estimator is suitable to the low-order method [18], but a direct extension to the arbitrary-order mimetic method [10], which is based on variable polynomial degree, may be cumbersome.

In this work, we develop a residual-based estimator for the virtual element method for diffusion problems in primal form [9]. This family of schemes is characterized by a general polynomial degree of accuracy m and a general regularity index $\alpha \in \mathbb{N}$, *i.e.*, the numerical approximations they provide belong to $C^\alpha(\Omega)$. The usefulness of developing methods with high regularity is discussed in reference [9]; for instance, it makes it possible to compute derived quantities of interest such as the fluxes. In the present paper we concentrate our attention on the C^1 case. Although the shape functions inside the elements are unknown, we are able to derive a residual-based error estimator by exploiting some specific characteristics of the method. Such estimator is the sum of local terms, each one of which being composed by three distinct parts associated with the residual (η^r), the approximation of the loading term (η^l) and the approximation of the bilinear form (η^c). A particularly interesting point in the present analysis is the term η^c, that gives a direct evaluation of the error that stems from the "virtual" approximation of the problem. Moreover we show that such term has a very natural and simple form direcly related to the "non consistent" part of the discrete bilinear form. In order to derive and analyze the proposed error estimator we need also to circumvent some technical difficulties related to the particular construction of the virtual method. For intance, we introduce projected (and thus computable also in the virtual setting) versions of the classical residual terms and derive inverse estimates for the virtual discrete space.

The paper is organized as follows. In Section 2 we present the mathematical model. In Section 3 we briefly review the virtual element method with arbitrary regularity [9] for $\alpha = 1$ and a general positive integer m. In Section 4 we introduce the a posteriori error estimator and we prove its reliability and efficiency in terms of the energy error. In Section 5 we show the performance of such estimator when it is combined with an adaptive strategy in the resolution of a set of model problems. Finally, in Section 6 we offer our final remarks and discusses the open issues for future work.

2. The mathematical model

Let us consider the Poisson problem for the scalar solution field u given by

$$-\Delta u = f \quad \text{in} \quad \Omega, \tag{2.1}$$

$$u = g \quad \text{on} \quad \partial\Omega, \tag{2.2}$$

where Ω is a bounded, open, polygonal subset of $\mathbb{R}^2$, f in $L^2(\Omega)$ is the forcing term, and g in $H^{\frac{1}{2}}(\partial\Omega)$ is the boundary datum. To ease the theoretical presentation, we consider the case of homogeneous Dirichlet boundary conditions, *i.e.*, $g = 0$ on $\partial\Omega$, while the more general case of non-homogeneous boundary conditions is investigated in the section of numerical experiments.

Throughout the paper, we follow the usual notation for Sobolev spaces, inner products and norms, see, *e.g.*, [24]. We also represent the set of polynomials defined on a generic control volume P that have degree less than or equal to the integer j by $\mathbb{P}_j(\mathsf{P})$ and the $L^2(\mathsf{P})$ orthogonal projection onto $\mathbb{P}_j(\mathsf{P})$ by π_j^{P}.

Let us now consider the functional space $H_0^1(\Omega) = \{v \in H^1(\Omega),\ v_{|\partial\Omega} = 0\}$. Problem (2.1)–(2.2) with $g = 0$ can be restated in the variational form:

find $u \in H_0^1(\Omega)$ *such that*

$$\mathcal{A}(u, v) = (f, v) \qquad \forall v \in H_0^1(\Omega), \tag{2.3}$$

where

$$\mathcal{A}(u, v) = \int_\Omega \nabla u \cdot \nabla v \, \mathrm{d}V \quad \text{and} \quad (f, v) = \int_\Omega f v \, \mathrm{d}V. \tag{2.4}$$

The bilinear form $\mathcal{A}$ is continuous and coercive and the linear functional $(f, \cdot)$ is continuous, thus implying the well-posedness of problem (2.3), *i.e.*, existence and uniqueness of the weak solution [27].

3. A C^1 VIRTUAL ELEMENT METHOD

Let $\{\Omega_h\}_h$ be a sequence of decompositions of Ω into elements P labeled by the mesh size parameter h. For the moment, we assume that each decomposition Ω_h is a finite number of *simple polygons*, *i.e.*, open simply connected subsets of Ω whose boundary is a non-intersecting line composed by a finite number of straight line segments. The precise assumption about the mesh regularity, which is required to perform the convergence analysis of the method, will be given in Section 3.7, see Assumption 1.

Let us consider the virtual element method with arbitrary regularity [9]. This method defines a family of mimetic schemes for each couple of integers (α, m), where $\alpha \geq 0$ is the *regularity index* and $m \geq \alpha + 1$ is the *consistency index*. All these schemes provide a numerical approximation to the solution of (2.3) that is C^α regular and $\mathcal{O}(h^m)$ accurate in the energy norm. In this paper we focus on the case $\alpha = 1$ and consider the family of mimetic schemes associated with each integer number $m \geq 2$ (see also Rem. 3.1). In the next subsections, for every h we will construct a finite dimensional space $V_h \subset H_0^1(\Omega)$, a family of bilinear forms $\mathcal{A}_h :\ V_h \times V_h \to \mathbb{R}$, which approximates the bilinear form $\mathcal{A}$, and a loading term, (f_h, v_h) (where f_h is a suitable approximation of f) which approximates the linear functional (f, v) in (2.4). The VEM method for the discretization of (2.3) reads as:

find $u_h \in V_h$ *such that:*

$$\mathcal{A}_h(u_h, v_h) = (f_h, v_h) \qquad \forall\, v_h \in V_h. \tag{3.1}$$

Remark 3.1. The same error estimator developed here immediately applies (with the same reliability proofs) also to the case $\alpha > 1$. Here, we prefer considering the case $\alpha = 1$ as this case is probably the most useful in applications.

3.1. Local discrete spaces

We denote a generic mesh vertex by v, a generic mesh edge by e and its length by $|\mathsf{e}|$, the area of polygon P by $|\mathsf{P}|$ and its boundary by $\partial\mathsf{P}$. The orientation of each edge e is reflected by the unit vector $\mathbf{n}_\mathsf{e}$, which is orthogonal to e and fixed once and for all. For any polygon P and any edge e of $\partial\mathsf{P}$, we define the unit normal vector $\mathbf{n}_{\mathsf{P},\mathsf{e}}$ that points out of P. We denote the set of mesh vertices by $\mathcal{V}_h$ and the set of mesh edges by $\mathcal{E}_h$.

For any integer $s \geq 0$ and any polygonal cell P, we consider the functional space of piecewise polynomials of degree s defined on the boundary $\partial\mathsf{P}$:

$$\mathbb{B}_s(\partial\mathsf{P}) := \left\{ v \in L^2(\partial\mathsf{P}) \ :\ v_{|\mathsf{e}} \in \mathbb{P}_s(\mathsf{e}),\ \forall \mathsf{e} \in \partial\mathsf{P} \right\}.$$

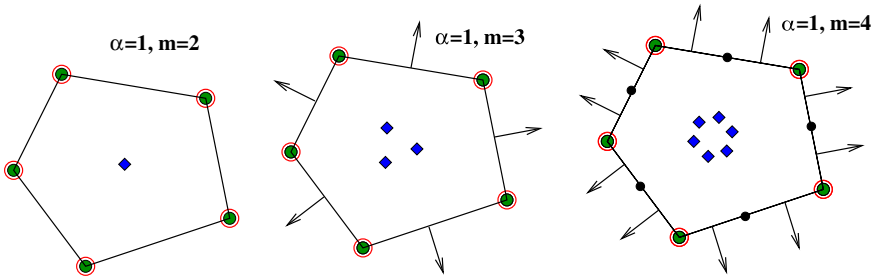

FIGURE 1. The degrees of freedom for $\alpha = 1$ and $m = 2, 3, 4$. The symbols shown in the plots represent the nodal values (dots) at the mesh vertices and edges, the first-order derivatives at the vertices (circles), the first-order normal derivatives at the mesh edges (arrows), and the internal moments (squares).

Let us introduce the integers $\alpha_0 := \max\{3, m\}$ and $\alpha_1 := \max\{1, m-1\}$. For any index $m \geq 2$, we consider the local finite element space associated with the polygonal cell P given by:

$$V_{h|\mathsf{P}} = \Big\{ v \in H^2(\mathsf{P}) \text{ with } \Delta^2 v \in \mathbb{P}_{m-2}(\mathsf{P}) \text{ s. t. } v_{|\partial\mathsf{P}} \in \mathbb{B}_{\alpha_0}(\partial\mathsf{P}),$$

$$\frac{\partial v}{\partial n}\Big|_{\partial\mathsf{P}} \in \mathbb{B}_{\alpha_1}(\partial\mathsf{P}), \nabla v_{|\partial\mathsf{P}} \in C^0(\partial\mathsf{P}) \Big\}, \tag{3.2}$$

where Δ^2 represents the biharmonic operator (see [9] for further explanations and details).

For example, for $m = 2$ we obtain the finite element space of functions in $H^2(\mathsf{P})$ such that:

- the trace on the boundary of P is continuous and is a piecewise polynomial of degree $\alpha_0 = 3$;
- the gradient on the boundary is continuous and the normal derivative on each edge is a polynomial of degree $\alpha_1 = 1$;
- in the interior of P, these functions satisfies the biharmonic equation $\Delta^2 v = p$ for some $p \in \mathbb{R}$.

Remark 3.2. The local space $V_{h|\mathsf{P}}$ in (3.2) is virtual in the sense that we do not need to build it explicitly for the practical implementation of the family of schemes here proposed.

3.2. Local degrees of freedom

We distinguish three kinds of degrees of freedom that are associated with each polygonal cell P:

- $\mathcal{V}_{\mathsf{P}}^h$: *vertex* degrees of freedom of P;
- $\mathcal{E}_{\mathsf{P}}^h$: *edge* degrees of freedom of P;
- $\mathcal{P}_{\mathsf{P}}^h$: *interior* degrees of freedom of P.

In Figure 1 we show the degrees of freedom for a pentagonal element for $\alpha = 1$ and $m = 2, 3, 4$.

Vertex degrees of freedom. The vertex degrees of freedom of the function v associated with the vertex v are the values of v and of the partial derivatives of v evaluated at v.

Edge degrees of freedom. The edge degrees of freedom of the function v are the values of v and of the normal derivatives of v evaluated at certain distinct points along e. More precisely, on each open edge e we consider the set of $\mathcal{N}_0^m$ distinct nodes $\{\mathbf{x}_i^0\}_{i=1,\ldots,\mathcal{N}_0^m}$ where $\mathcal{N}_0^m = \max(m-3, 0)$. The nodal degrees of freedom of v associated with edge e are given by $v(\mathbf{x}_i^0)$, *i.e.*, the values of v at $\mathbf{x}_i^0$. We also consider the set of $\mathcal{N}_1^m$ distinct

nodes $\{\mathbf{x}_i^1\}_{i=1,\dots,\mathcal{N}_1^m}$ where $\mathcal{N}_1^m = \max(m-2,0)$. The normal derivative degrees of freedom of v associated with edge e are given by $\partial v(\mathbf{x}_i^1)/\partial n$, *i.e.*, the normal derivative of v at $\mathbf{x}_i^1$. The points of the sets $\{\mathbf{x}_i^0\}_i$ and $\{\mathbf{x}_i^1\}_i$ can be uniformly spaced along e or chosen as the nodes of some integration rule like those provided by Gauss–Lobatto formulas [10].

Internal degrees of freedom. The internal degrees of freedom of the function v are the polynomial moments of v defined with respect to a certain basis of the local space of polynomials of degree up to $m-2$ on P. More precisely, let $\mathbf{s} = (s_1, s_2)$ with $s_1, s_2 \geq 0$ be a two-dimensional multi-index with the usual notation $|\mathbf{s}| := s_1 + s_2$ and $\mathbf{x}^{\mathbf{s}} = x_1^{s_1} x_2^{s_2}$ when $\mathbf{x} = (x_1, x_2)$. We consider the set of $m(m-1)/2$ monomials

$$\mathcal{M}_{m-2} = \left\{ \left(\frac{\mathbf{x} - \mathbf{x}_\mathsf{P}}{h_\mathsf{P}} \right)^{\mathbf{s}}, \, |\mathbf{s}| \leq m-2 \right\}, \tag{3.3}$$

which is a basis for the local polynomial space $\mathbb{P}_{m-2}(\mathsf{P})$. The *internal degrees of freedom* of a function v are the $m(m-1)/2$ moments:

$$\frac{1}{|\mathsf{P}|} \int_\mathsf{P} q(\mathbf{x})\, v(\mathbf{x}) \, \mathrm{d}V \qquad \forall q \in \mathcal{M}_{m-2}(\mathsf{P}).$$

Remark 3.3. On each edge e, the degrees of freedom $\mathcal{V}_\mathsf{P}^h$ plus $\mathcal{E}_\mathsf{P}^h$ uniquely determine a polynomial of degree α_0 on each edge e of P representing the function value, and a polynomial of degree α_1, representing the normal derivative. Thus, prescribing the degrees of freedom $\mathcal{V}_\mathsf{P}^h$ plus $\mathcal{E}_\mathsf{P}^h$ is equivalent to prescribing v and $\partial v/\partial n$ on $\partial\mathsf{P}$. On the other hand, prescribing the degrees of freedom $\mathcal{P}_\mathsf{P}^h$ is equivalent to prescribing the L^2-orthogonal projection $\pi_{m-2}^\mathsf{P}(v)$ onto the space of the polynomials of degree up to $m-2$ defined on P.

Remark 3.4. As pointed out in reference [9], a better condition number of the stiffness matrix is obtained by scaling the nodal degrees of freedom by an appropriate local mesh size factor.

For the space $V_{h|\mathsf{P}}$ and the degrees of freedom $\mathcal{V}_\mathsf{P}^h$ plus $\mathcal{E}_\mathsf{P}^h$ plus $\mathcal{P}_\mathsf{P}^h$ we have the following *unisolvence result*, whose proof is found in [9].

Proposition 3.5. *Let P be a simple polygon with $N_\mathsf{P}^{\mathcal{E}_h}$ edges, and the space $V_{h|\mathsf{P}}$ be generated by the monomials in (3.2). The degrees of freedom $\mathcal{V}_\mathsf{P}^h$ plus $\mathcal{E}_\mathsf{P}^h$ plus $\mathcal{P}_\mathsf{P}^h$ are unisolvent for $V_{h|\mathsf{P}}$.*

3.3. Construction of the finite element space $\mathbf{V_h}$

We can now design V_h, the *virtual element space* on the whole domain Ω. For every decomposition Ω_h of Ω into simple polygons P we first define the *space without boundary conditions*:

$$W_h = \{ v \in H^2(\Omega) \ : \ v_{|\mathsf{P}} \in V_{h|\mathsf{P}} \ \forall \mathsf{P} \in \Omega_h \}. \tag{3.4}$$

In agreement with the *local choice* of the degrees of freedom of the previous subsection, in W_h we choose the following *global* degrees of freedom:

- $\mathcal{V}^h$: the value of v_h and ∇v_h at the vertices of $\mathcal{V}_h$;
- $\mathcal{E}^h$: the value of v_h and of $\partial v_h/\partial n$ at, respectively, the $\mathcal{N}_0^m$ and $\mathcal{N}_1^m$ internal nodes defined in Section 3.2 for each edge e of $\mathcal{E}_h$;
- $\mathcal{P}^h$: the value of the moments

$$\frac{1}{|\mathsf{P}|} \int_\mathsf{P} q(\mathbf{x}) v_h(\mathbf{x}) \, \mathrm{d}V \qquad \forall q \in \mathcal{M}_{m-2}(\mathsf{P})$$

in each polygonal cell P.

Finally, the discrete space $V_h = W_h \cap H^1_0(\Omega)$ is given by

$$V_h = \Big\{ v \in H^2(\Omega) \ : \ v_{|\mathsf{P}} \in V_{h|\mathsf{P}} \ \forall \mathsf{P} \in \Omega_h, \ v_{|\partial\Omega} = 0 \Big\}. \tag{3.5}$$

Note that the condition $v_h \in V_h$ implies $v_h = 0$ on the vertices and the edges of the boundary $\partial\Omega$. Therefore, the degrees of freedom of V_h are simply the ones introduced above, excluding the nodal degrees of freedom associated with the function values (but not the derivatives) of the boundary vertices and edges.

3.4. Construction of $\mathcal{A}_h$

We build the discrete bilinear form $\mathcal{A}_h$ by assembling the local bilinear forms $\mathcal{A}_{h,\mathsf{P}}$ in accordance with

$$\mathcal{A}_h\big(w_h, v_h\big) = \sum_{\mathsf{P}\in\Omega_h} \mathcal{A}_{h,\mathsf{P}}\big(w_h, v_h\big) \qquad \forall w_h, v_h \in V_h. \tag{3.6}$$

The local bilinear forms $\mathcal{A}_{h,\mathsf{P}}$ are all *symmetric* and satisfy the following fundamental properties of *consistency*, *stability and continuity*.

- **Consistency:** for all h and for all P in Ω_h it holds

$$\mathcal{A}_{h,\mathsf{P}}\big(p, v_h\big) = \mathcal{A}_{\mathsf{P}}\big(p, v_h\big) \qquad \forall p \in \mathbb{P}_m(\mathsf{P}), \ \forall v_h \in V_{h|\mathsf{P}}. \tag{3.7}$$

  where

$$\mathcal{A}_{\mathsf{P}}\big(p, v_h\big) = \int_{\mathsf{P}} \nabla p \cdot \nabla v_h \, \mathrm{d}V.$$

- **Stability**: there exist two positive constants α_* and α^*, independent of h and P, such that

$$\alpha_* \, \mathcal{A}_{\mathsf{P}}\big(v_h, v_h\big) \le \mathcal{A}_{h,\mathsf{P}}\big(v_h, v_h\big) \le \alpha^* \, \mathcal{A}_{\mathsf{P}}\big(v_h, v_h\big) \qquad \forall v_h \in V_{h|\mathsf{P}}. \tag{3.8}$$

  For simplicity, we will refer to the "*Stability and Continuity*" property using the single-word label "*Stability*".

Let us assume that condition (3.7) is true and integrate by parts:

$$\begin{aligned} \mathcal{A}_{h,\mathsf{P}}\big(p, v_h\big) &= \int_{\mathsf{P}} \nabla p \cdot \nabla v_h \, \mathrm{d}V \\ &= -\int_{\mathsf{P}} (\Delta p) \, v_h \, \mathrm{d}V + \int_{\partial\mathsf{P}} v_h \, \mathbf{n}_{\mathsf{P}} \cdot \nabla p \, \mathrm{d}S. \end{aligned} \tag{3.9}$$

Since $\Delta p \in \mathbb{P}_{m-2}(\mathsf{P})$, the first integral in the right-hand side of (3.9) can be expressed through the polynomial moments of v_h, and can, thus, be computed exactly by using its internal degrees of freedom. On the other hand, it holds that $(\mathbf{n}_{\mathsf{P}} \cdot \nabla p) \in \mathbb{P}_{m-1}(\mathsf{e})$ and $v_{h|\mathsf{e}} \in \mathbb{P}_{\alpha_0}(\mathsf{e})$ for all $\mathsf{e} \subset \partial\mathsf{P}$, so that the second integral in the right-hand side of (3.9) can be computed exactly. Therefore, the right hand side of (3.7) can be computed explicitly without knowing v_h in the interior of P. We formally summarize this result for future reference in the paper in the following remark.

Remark 3.6. The local degrees of freedom allow us to compute exactly $\mathcal{A}_{h,\mathsf{P}}\big(p, v_h\big)$ for any $p \in \mathbb{P}_m(\mathsf{P})$ and for any $v_h \in V_{h|\mathsf{P}}$.

We are left to show how to construct a computable $\mathcal{A}_h$ that satisfies (3.7) and (3.8). We review such construction in Section 3.6 and we refer the reader interested to alternative possibilities to [9, 11].

3.5. Construction of the loading term

Let us define the function f_h on each element P of Ω_h as the $L^2(\mathsf{P})$-projection of the function f onto the space $\mathbb{P}_{m-2}(\mathsf{P})$, that is,

$$f_h = \pi^{\mathsf{P}}_{m-2}(f) \qquad \text{on each } \mathsf{P} \in \Omega_h.$$

The loading term can be written as

$$\begin{aligned}(f_h, v_h) &= \sum_{\mathsf{P}\in\Omega_h} \int_{\mathsf{P}} f_h\, v_h \,\mathrm{d}V = \sum_{\mathsf{P}\in\Omega_h} \int_{\mathsf{P}} \pi^{\mathsf{P}}_{m-2}(f)\, v_h \,\mathrm{d}V \\ &= \sum_{\mathsf{P}\in\Omega_h} \int_{\mathsf{P}} \pi^{\mathsf{P}}_{m-2}(f)\, \pi^{\mathsf{P}}_{m-2}(v_h) \,\mathrm{d}V = \sum_{\mathsf{P}\in\Omega_h} \int_{\mathsf{P}} f\, \pi^{\mathsf{P}}_{m-2}(v_h) \,\mathrm{d}V\end{aligned}$$

where the last two identities follows from the fact that v_h and $\pi^{\mathsf{P}}_{m-2}(v_h)$ have the same internal moments and $\pi^{\mathsf{P}}_{m-2}(f)$ is the L^2 orthogonal projection of f onto $\mathbb{P}_{m-2}(\mathsf{P})$. Thus, the right-hand side of (3.1) can be computed exactly by using the degrees of freedom of the functions in V_h that represent the internal moments.

3.6. Implementation of the local stiffness matrices

In this section, we briefly review the construction of the local stiffness matrix M_{P}, which is associated with the local bilinear form $\mathcal{A}_{h,\mathsf{P}}$, following the general guidelines in [14].

Let n_{P} denote the dimension of the local space $\mathcal{V}^h_{\mathsf{P}}$. For each polygonal cell $\mathsf{P} \in \Omega_h$, the elemental stiffness matrix $\mathsf{M}^{\mathrm{VEM}}_{\mathsf{P}} \in \mathbb{R}^{n_{\mathsf{P}}\times n_{\mathsf{P}}}$ is such that

$$\mathcal{A}_{h,\mathsf{P}}\big(w_{h,\mathsf{P}}, v_{h,\mathsf{P}}\big) = \underline{w}^T_{h,\mathsf{P}}\, \mathsf{M}^{\mathrm{VEM}}_{\mathsf{P}}\, \underline{v}_{h,\mathsf{P}} \qquad \forall w_{h,\mathsf{P}},\ v_{h,\mathsf{P}} \in V_{h|\mathsf{P}},$$

where the vectors $\underline{w}_{h,\mathsf{P}}$ and $\underline{v}_{h,\mathsf{P}}$ represents the values of the local degrees of freedom of $w_{h,\mathsf{P}}$ and $v_{h,\mathsf{P}}$. The global stiffness matrix is then obtained by a standard finite element-like assembly procedure.

Let χ_i be the function that returns the ith degree of freedom of its argument, and $\{\psi_i\}_{i=1}^{n_{\mathsf{P}}}$ the set of "canonical" basis function of the local virtual space $V_{h|\mathsf{P}}$, *e.g.*, $\chi_i(\psi_j) = 1$ if $i = j$ and 0 if $i \neq j$. We enumerate the whole set of $m_{\mathsf{P}} = (m+1)(m+2)/2$ scaled monomials that are used to define the degrees of freedom in Section 3.1 by the local indices i and j (resp., m_i and m_j).

To compute the stiffness matrix, we need two auxiliary matrices B and D, which are defined as follows. The jth column of matrix B, for $j = 1, \dots, n_{\mathsf{P}}$, is defined by

$$\mathsf{B}_{1j} = \begin{cases} \displaystyle\int_{\partial\mathsf{P}} \psi_j \,\mathrm{d}S & \text{if } m = 1, \\ \displaystyle\int_{\mathsf{P}} \psi_j \,\mathrm{d}V & \text{if } m \geq 2, \end{cases} \tag{3.10}$$

$$\mathsf{B}_{ij} = \int_{\mathsf{P}} \nabla m_i \cdot \nabla \psi_j \,\mathrm{d}V, \quad i = 2, \dots, m_{\mathsf{P}}. \tag{3.11}$$

The jth column of matrix D, for $j = 1, \dots, m_{\mathsf{P}}$, collects the degrees of freedom of the jth monomials and is defined by:

$$\mathsf{D}_{ij} = \chi_i(m_j), \qquad i = 1, \dots, n_{\mathsf{P}}. \tag{3.12}$$

Note that the matrices B, D are explicitly computable. In particular, the terms in (3.11) can be easily computed recalling the integration by parts

$$\int_{\mathsf{P}} \nabla m_i \cdot \nabla \psi_j \,\mathrm{d}V = -\int_{\mathsf{P}} \psi_j(\Delta m_i) \,\mathrm{d}V + \int_{\partial\mathsf{P}} \psi_j(\mathbf{n}_{\mathsf{P}} \cdot \nabla m_i) \,\mathrm{d}S$$

and using the degrees of freedom values of ψ_j.

Then, we consider the matrices $\mathsf{G} = \mathsf{B}\mathsf{D}$, $\boldsymbol{\Pi}^a = \mathsf{D}\mathsf{G}^{-1}\mathsf{B}$ and $\widetilde{\mathsf{G}}$, which is obtained from matrix G by setting its first row to zero. The VEM stiffness matrix $\mathsf{M}_\mathsf{P}^{\mathrm{VEM}}$ is the sum of two matrices, defined by the following formula:

$$\mathsf{M}_\mathsf{P}^{\mathrm{VEM}} = (\mathsf{G}^{-1}\mathsf{B})^T\widetilde{\mathsf{G}}(\mathsf{G}^{-1}\mathsf{B}) + (\mathsf{I} - \boldsymbol{\Pi}^a)^T\mathsf{S}(\mathsf{I} - \boldsymbol{\Pi}^a), \tag{3.13}$$

where I is the identity matrix and S is a symmetric and positive definite matrix. The first matrix term corresponds to the consistency property and the second term ensures stability. According to [11], we can set $\mathsf{S} = \mathsf{I}$, the identity matrix. Nonetheless, the choice of S is not unique and, therefore, we have a family of virtual element schemes that differ by this matrix.

3.7. *A priori* error estimates

Let us introduce the following mesh assumptions.

Assumption 1 (Mesh regularity)**.** There exists a real number $\gamma > 0$ such that, for all h, each element P in Ω_h is star-shaped with respect to a ball of radius $\geq \gamma h_\mathsf{P}$, where h_P is the diameter of P. Moreover, there exists a real number $\gamma' > 0$ such that, for all h and for each element P in Ω_h, the distance between any two vertices of P is $\geq \gamma' h_\mathsf{P}$.

Then, the following convergence theorem holds, see reference [9] for the proof.

Theorem 3.7. *Let the consistency and stability conditions* (3.7)–(3.8) *and the mesh assumptions considered above hold. Then, the discrete problem* (3.1) *has a unique solution and, if the solution u of* (2.3) *belongs to $W^{1,\infty}(\Omega)$, it holds that*

$$||u - u_h||_{H^1(\Omega)} \leq C \sum_{\mathsf{P}\in\Omega_h} h_\mathsf{P}^s\, |u|_{H^{s+1}(\mathsf{P})} \tag{3.14}$$

for all $1 \leq s \leq m$, where C is a constant independent of h.

The condition $u \in W^{1,\infty}(\Omega)$ can be relaxed [9].

4. A reliable and efficient error estimator

In this section we first present the error estimator, then prove its reliability and efficiency. Through the rest of the paper we will assume the mesh conditions introduced in Section 3.7.

4.1. The error estimator

In order to introduce the error estimator we need a few preliminary definitions. We start by introducing, for all $\mathsf{P} \in \Omega_h$, the following energy projection $\Pi_m^\mathsf{P} : H^1(\mathsf{P}) \to \mathbb{P}_{m,0}(\mathsf{P})$, where $\mathbb{P}_{m,0}$ indicates the subpace of $\mathbb{P}_m$ of polynomials with zero average. For all $v \in H^1(\mathsf{P})$, the image $\Pi_m^\mathsf{P} v \in \mathbb{P}_{m,0}(\mathsf{P})$ is uniquely defined as the energy projection

$$\mathcal{A}_\mathsf{P}\big(\Pi_m^\mathsf{P} v, p\big) = \mathcal{A}_\mathsf{P}\big(v, p\big) \qquad \forall p \in \mathbb{P}_{m,0}(\mathsf{P}). \tag{4.1}$$

Due to the consistency condition (3.7) together with the symmetry of both $\mathcal{A}_\mathsf{P}$ and $\mathcal{A}_{h,\mathsf{P}}$, if $v_h \in V_{h|\mathsf{P}} \subset H^1(\mathsf{P})$, then (4.1) is equivalent to

$$\mathcal{A}_{h,\mathsf{P}}\big(\Pi_m^\mathsf{P} v_h, p\big) = \mathcal{A}_{h,\mathsf{P}}\big(v_h, p\big) \qquad \forall p \in \mathbb{P}_{m,0}(\mathsf{P}). \tag{4.2}$$

Therefore, $\Pi_m^\mathsf{P} v_h$ is explicitly computable for any function $v_h \in V_{h|\mathsf{P}}$.

Now, let us recall that π_m^P represents the $L^2(\mathsf{P})$ projection on $\mathbb{P}_m(\mathsf{P})$. For all $v_{h,\mathsf{P}} \in V_{h|\mathsf{P}}$ and $\mathsf{P} \in \Omega_h$ the projection $\pi_m^\mathsf{P}\, \Delta v_h$ is explicitly computable. Indeed, integrating twice by parts, for all $p \in \mathbb{P}_m(\mathsf{P})$ it holds

$$\int_\mathsf{P} (\Delta v_{h,\mathsf{P}}) p \,\mathrm{d}V = \int_\mathsf{P} v_{h,\mathsf{P}} \Delta p \,\mathrm{d}V + \int_{\partial\mathsf{P}} p\, \mathbf{n}_\mathsf{P} \cdot \nabla v_{h,\mathsf{P}} \,\mathrm{d}S - \int_{\partial\mathsf{P}} v_{h,\mathsf{P}}\, \mathbf{n}_\mathsf{P} \cdot \nabla p \,\mathrm{d}S. \tag{4.3}$$

The first term in the right hand side is computable using the internal degrees of freedom (moments) of v_h since $\Delta p \in \mathbb{P}_{m-2}(\mathsf{P})$. The remaining terms involve the trace of v_h and of its normal derivative along the polygonal boundary $\partial\mathsf{P}$, which are known explicitly, see Section 3.1.

We can now introduce, for all $\mathsf{P} \in \Omega_h$, the following *local* and *computable* terms:

$$\eta_{\mathsf{P}}^r = h_{\mathsf{P}} \| f + \pi_m^{\mathsf{P}}(\Delta u_{h,\mathsf{P}}) \|_{L^2(\mathsf{P})}, \tag{4.4}$$

$$\eta_{\mathsf{P}}^l = h_{\mathsf{P}} \| f - f_h \|_{L^2(\mathsf{P})}, \tag{4.5}$$

$$\eta_{\mathsf{P}}^c = \mathcal{A}_{h,\mathsf{P}}\big(u_{h,\mathsf{P}} - \Pi_m^{\mathsf{P}} u_{h,\mathsf{P}}, u_{h,\mathsf{P}} - \Pi_m^{\mathsf{P}} u_{h,\mathsf{P}}\big)^{1/2}, \tag{4.6}$$

where u_h is the solution of the discrete problem and $u_{h,\mathsf{P}}$ its restriction to the generic element P.

The first term, where a kind of discrete residual appears, represents an estimation of the error stemming from the Galerkin discretization of the problem. The second term estimates the right hand side approximation. The third term bounds the error related to the inconsistency between the continuous and discrete bilinear forms, $\mathcal{A}$ and $\mathcal{A}_h$.

The result here below shows the reliability of the proposed error estimator η; the proof is postponed to the next subsection.

Theorem 4.1. *Let u_h be the solution of (3.1) and u the solution of (2.3). Let the global error estimator*

$$\eta^2 = \sum_{\mathsf{P}\in\Omega_h} \eta_{\mathsf{P}}^2, \qquad \textit{where} \qquad \eta_{\mathsf{P}}^2 = (\eta_{\mathsf{P}}^r)^2 + (\eta_{\mathsf{P}}^l)^2 + (\eta_{\mathsf{P}}^c)^2 \quad \forall \mathsf{P} \in \Omega_h.$$

Then, under Assumption 1 on the regularity of the meshes, there exists a constant C independent of h such that

$$\|u - u_h\|_{H^1(\Omega)} \le C\eta.$$

Since the above estimator η^2 is the sum of local terms, it can be used for an adaptive mesh generation strategy, as will be shown in the section of the numerical tests. Note that, differently from standard FEM residual estimators, there are no jump terms since the solution u_h is globally C^1.

The present error estimator can be easily generalized to the case of the Poisson problem. Indeed, let us consider the more general bilinear form

$$\mathcal{A}(u,v) = \int_\Omega K\nabla u \cdot \nabla v \, \mathrm{d}V \tag{4.7}$$

with a uniformly positive diffusion tensor $K \in [L^\infty(\Omega)]^{2\times 2}$, which we assume to be piecewise constant with respect to the mesh Ω_h. In the presence of jumps in the material data, it may be convenient to locally relax the continuity requirements in v_h and allow for (only) C^0 continuity across selected edges of the mesh [9]. This is easily achieved by considering the same degrees of freedom for each element P, but those associated with derivatives at the nodes of the chosen edges (extrema included) are no longer single-valued and may take different values when referred to different elements. This strategy requires to modify only the assembly of the global stiffness matrix while the construction of the local element matrices remains unchanged. Following the proof shown in Section 4.2, it is easy to check that in such a case the error estimator must be simply modified as follows.

(1) The residual term of the estimator must be changed as

$$\eta_{\mathsf{P}}^r = h_{\mathsf{P}} \| f + \pi_m^{\mathsf{P}} \left(\operatorname{div}\left(K\nabla u_{h,\mathsf{P}}\right)\right) \|_{L^2(\mathsf{P})} \qquad \forall \mathsf{P} \in \Omega_h.$$

Using a double integration by parts analogous to (4.3) immediately shows that $\pi_m^{\mathsf{P}} \left(\operatorname{div}\left(K\nabla u_{h,\mathsf{P}}\right)\right)$ is explicitly computable for all $\mathsf{P} \in \Omega_h$.

(2) The estimator must be enriched by adding the computable jump term

$$\sum_{\mathsf{P}\in\Omega_h} (\eta^j_{\mathsf{P}})^2 \quad \text{with} \quad (\eta^j_{\mathsf{P}})^2 = \frac{1}{2} \sum_{\mathsf{e}\in\partial\mathsf{P}\cap J_h} h_{\mathsf{P}} \left\| \left[\!\left[K\nabla u_h \cdot \mathbf{n}_{\mathsf{e}} \right]\!\right] \right\|^2_{L^2(\mathsf{e})},$$

where $[\![\cdot]\!]$ denotes the standard jump operator and $J_h \subset \mathcal{E}_h$ is the subset of mesh edges across which v_h is only of C^0 regularity and/or jumps of the material data K occur.

With arguments that are similar to the original case, one can easily prove also the following result.

Corollary 4.2. *Let u_h be the solution of (3.1) and u the solution of (2.3), for the case with the more general bilinear form (4.7) and piecewise constant coefficients K. Let η be the error estimator presented in Theorem 4.1, with the two modifications above. Then, under Assumption 1 on the regularity of the meshes, there exists a constant C independent of h (but depending on $||K||_{L^\infty(\Omega)}$ and $||K^{-1}||_{L^\infty(\Omega)}$) such that*

$$\|u - u_h\|_{H^1(\mathsf{P})} \leq C\eta.$$

Remark 4.3. We note that the constants appearing above are uniform in the mesh size but not explicitly known. Another interesting (and different) approach would be that of developing guaranteed error estimators, that need the solution of auxiliary (local) problems but give an explicit value of all the constants involved, see for instance the recent paper [39] and citations therein.

Remark 4.4. We end this section with an important observation regarding the consistency of the error estimator η^c_{P}. The term η^c_{P} can be computed in a very direct way, in accordance with the stiffness matrix construction discussed in Section 3.6. Indeed, by writing (4.2) and (4.6) in terms of matrices, using Definition (3.13) one can derive

$$(\eta^c_{\mathsf{P}})^2 = \underline{u}^T_{h,\mathsf{P}} \, (\mathsf{I} - \boldsymbol{\Pi}^a)^T \mathsf{S} (\mathsf{I} - \boldsymbol{\Pi}^a) \, \underline{u}_{h,\mathsf{P}}$$

where we recall that $\underline{u}_{h,\mathsf{P}}$ represents the local degree of freedom of $u_{h,\mathsf{P}}$.

4.2. Proof of Theorem 4.1

In this section we show the proof of Theorem 4.1. We will make use of the following two lemmas. In general, we cannot apply the standard scaling arguments since the functions of $V_{h|\mathsf{P}}$ are not associated with a fixed reference space (independent of P) on some reference element.

Lemma 4.5. *It exists a constant C independent of h such that*

$$h_{\mathsf{P}} |v_h|_{H^2(\mathsf{P})} \leq C \, |v_h|_{H^1(\mathsf{P})} \qquad \forall \mathsf{P} \in \Omega_h, \ \forall v_h \in V_{h|\mathsf{P}}. \tag{4.8}$$

Proof. We follow here a generalized scaling argument in the spirit of [7, 32]. In view of Assumption 1, all the polygonal elements in $\{\Omega_h\}_h$ have at most $N^{\mathcal{E}_h}$ edges and $N^{\mathcal{E}_h}$ is independent of h. Therefore, it is not restrictive to assume that the number of edges n of each polygonal cell with $3 \leq n \leq N^{\mathcal{E}_h}$ is fixed. Given any polygon P of the mesh family with n edges and vertices, let $X = \{X_1, X_2, \ldots, X_n\}$ represent the position of the n (anti-clockwise) vertices defining $\mathsf{P} = \mathsf{P}(X)$. Since inequality (4.8) scales with the size of the element, it is not restrictive to assume that the diameter $h_{\mathsf{P}} = 1$ and, by a simple translation, that $X_1 = (0, 0)$. Since the space $V_{h|\mathsf{P}}$ is finite dimensional, it holds that:

$$|v_h|_{H^2(\mathsf{P})} \leq C \, |v_h|_{H^1(\mathsf{P})} \qquad \forall v_h \in V_{h|\mathsf{P}}, \tag{4.9}$$

where the factor $C = C(X)$ depends on X.

Due to the diameter property above, the set Σ of vectors $X \in \mathbb{R}^{2n}$ representing all possible scaled polygons P with n edges and $X_1 = (0, 0)$ constitutes a bounded set. Moreover, Σ is also closed, and, hence, a compact set.

In fact, property $h_{\mathsf{P}} = 1$ combined with Assumption 1 does not allow the vectors in Σ to be arbitrarily close to inadmissible vectors $\bar{X} \notin \Sigma$ that do not correspond to a (non-degenerate) polygon. For instance, $h_{\mathsf{P}} = 1$ combined with the second condition in Assumption 1 implies that any two vertexes of the polygon must be at least at distance γ', thus preventing convergence to degenerate polygons where two vertices are collapsed into a single vertex. Therefore, if $C(X)$ is the factor in (4.9) associated with the element P defined by X, we need to show that the function

$$C(X) = \max_{v_h \in V_{h|\mathsf{P}}/\mathbb{R}} \frac{h_{\mathsf{P}} |v_h|_{H^2(\mathsf{P})}}{|v_h|_{H^1(\mathsf{P})}} \tag{4.10}$$

is a continuous function of X. The maximum of $C(X)$ on Σ is the constant appearing in (4.8). Note that in equation (4.10), although we can assume $h_{\mathsf{P}} = 1$, we prefer to keep the term h_{P} for better clarity in the following.

Now, let $\{X_k\}$, $k \in \mathbb{N}$, be any convergent sequence to X and P_k be the polygonal cell associated with X_k, Clearly, $\mathsf{P}_k \to \mathsf{P}$ as k tends to ∞. To prove that $C(X)$ is continuous with respect to X we need to show that $\lim_{k\to\infty} C(X_k) = C(X)$. Let v_h be the function in $V_{h|\mathsf{P}}$ that achieves the maximum in (4.10). For every k, we consider the degrees of freedom defined on P_k and P with respect to the corresponding vertices and edges. Then, we consider the function $v_h^k \in V_{h|\mathsf{P}_k}$ whose degrees of freedom on the element P_k have the same value as the corresponding ones of v_h on P. Moreover, for k sufficiently large, it can always be built a sequence ϕ^k of $W^{2,\infty}$ invertible mappings from P to P_k, such that ϕ^k converge to the identity (in $W^{2,\infty}$) as $k \to \infty$. Using such mappings it can then be shown that, as $X_k \to X$, the seminorms $|v_h^k|_{H^s(\mathsf{P}_k)} \to |v_h|_{H^s(\mathsf{P})}$, $s = 1, 2$. This can be done by checking that $v_h^k \circ \phi^k$ converges to v_h in $H^2(\mathsf{P})$. Without showing the details, such simple calculation involves writing the biharmonic variational problem associated with the definition of $V_{h|\mathsf{P}}$ and $V_{h|\mathsf{P}_k}$, a change of variables through the mapping ϕ^k, and noting that $\{\phi^k\}_k$ converge to the identity in $W^{2,\infty}$ as $X^k \to X$. Since $|v_h^k|_{H^s(\mathsf{P}_k)} \to |v_h|_{H^s(\mathsf{P})}$ for $s = 1, 2$, the construction above immediately implies that

$$\lim_{k\to\infty} C(X_k) \geq \lim_{k\to+\infty} \frac{h_{\mathsf{P}} |v_h^k|_{H^2(\mathsf{P})}}{|v_h^k|_{H^1(\mathsf{P})}} = C(X).$$

The converse is shown with an analogous reasoning in the opposite direction. □

With a similar argument also the following inverse estimate, useful in the proof of the next Lemma, can be shown:

$$h_{\mathsf{P}} |v_h|_{H^1(\mathsf{P})} \leq C \, \|v_h\|_{L^2(\mathsf{P})} \qquad \forall \mathsf{P} \in \Omega_h, \ \forall v_h \in V_{h|\mathsf{P}}. \tag{4.11}$$

Lemma 4.6. *It exists a Clément-type interpolant $H_0^1(\Omega) \to \mathcal{V}^h$ such that for any function $v \in H_0^1(\Omega)$ and all $\mathsf{P} \in \Omega_h$, the interpolant $v_{\mathfrak{C}}$ satisfies*

$$\|v - v_{\mathfrak{C}}\|_{L^2(\mathsf{P})} + h_{\mathsf{P}} |v_{\mathfrak{C}}|_{H^1(\mathsf{P})} \leq C h_{\mathsf{P}} |v|_{H^1(\omega_{\mathsf{P}})} \tag{4.12}$$

with C independent of h and where ω_{P} is the union of all elements P that share a vertex with P.

Proof. Let the subspace $\widehat{V}_h \subset \mathcal{V}^h$ be defined as the space of all functions in $\mathcal{V}^h$ such that the value of all the degrees of freedom associated with the pointwise derivatives and the first- or higher-order moments are zero. Let Ξ_h denote the set of the vertices and the edge nodes of Ω_h associated with the degrees of freedom that are defined through a pointwise evaluations, *i.e.*, the set of all the nodes associated with $\mathcal{V}^h$ and $\mathcal{E}^h$ for the derivative order $j = 0$. Then, given any $v \in H_0^1(\Omega)$, we define $v_{\mathfrak{C}} \in \widehat{V}_h$ by

$$\begin{cases} v_{\mathfrak{C}}(\nu) = \dfrac{1}{|\omega_\nu|} \displaystyle\int_{\omega_\nu} v \, \mathrm{d}V \qquad \forall \nu \in \Xi_h, \\ \dfrac{1}{|\mathsf{P}|} \displaystyle\int_{\mathsf{P}} v_{\mathfrak{C}} \, \mathrm{d}V = \dfrac{1}{|\mathsf{P}|} \displaystyle\int_{\mathsf{P}} v \, \mathrm{d}V \qquad \forall \mathsf{P} \in \Omega_h, \end{cases} \tag{4.13}$$

where the symbol ν indicates a generic vertex and

$$\omega_\nu = \{\cup \mathsf{P} \,:\, \nu \in \partial \mathsf{P}\}.$$

Note that, for all $\mathsf{P} \in \Omega_h$, if $v : \omega_\mathsf{P} \to \mathbb{R}$ is constant, then $v_\mathfrak{C}|_\mathsf{P} = v|_\mathsf{P}$; the above operator preserves local constants. Assume, for the moment, that the following continuity property holds

$$\|v_\mathfrak{C}\|_{L^2(\mathsf{P})} \le C\|v\|_{L^2(\omega_\mathsf{P})} \qquad \forall \mathsf{P} \in \Omega_h,\ \forall v \in H^1_0(\Omega), \tag{4.14}$$

with a constant factor C independent of h and $\mathsf{P} \in \Omega_h$. Then, for all $v \in H^1_0(\Omega)$ and $\mathsf{P} \in \Omega_h$, let $\overline{v}$ denote the average of v on ω_P. First by a triangle inequality and recalling that the operator preserves constants, then using (4.14), finally by standard approximation estimates on star shaped domains, we get

$$\begin{aligned}\|v - v_\mathfrak{C}\|_{L^2(\mathsf{P})} &\le \|v - \overline{v}\|_{L^2(\mathsf{P})} + \|(v-\overline{v})_\mathfrak{C}\|_{L^2(\mathsf{P})} \\ &\le C\|v - \overline{v}\|_{L^2(\omega_\mathsf{P})} \le Ch_\mathsf{P}|v|_{H^1(\omega_\mathsf{P})},\end{aligned}$$

which is a part of (4.12). The remaining part follows by using again the constant preserving property, inverse estimate (4.11), bound (4.14) and standard approximation properties

$$\begin{aligned}|v_\mathfrak{C}|^2_{H^1(\mathsf{P})} = |(v-\overline{v})_\mathfrak{C}|^2_{H^1(\mathsf{P})} &\le C(h_\mathsf{P})^{-2}\|(v-\overline{v})_\mathfrak{C}\|^2_{L^2(\mathsf{P})} \\ &\le C(h_\mathsf{P})^{-2}\|v-\overline{v}\|^2_{L^2(\omega_\mathsf{P})} \le C|v|^2_{H^1(\omega_\mathsf{P})}.\end{aligned}$$

To conclude the proof, we are left to show inequality (4.14). From the definition of $v_\mathfrak{C}$ it follows that

$$|\mathsf{P}|\left(\sum_{\nu\in\Xi_h\cap\partial\mathsf{P}} |v_\mathfrak{C}(\nu)|^2 + \left|\frac{1}{|\mathsf{P}|}\int_\mathsf{P} v_\mathfrak{C}\,\mathrm{d}V\right|^2\right) \le C\|v\|^2_{L^2(\omega_\mathsf{P})}$$

for all $\mathsf{P} \in \Omega_h$, $v \in H^1_0(\Omega)$. Inequality (4.14) follows if there exists a constant C independent of h such that

$$\|v_h\|^2_{L^2(\mathsf{P})} \le C\ |\mathsf{P}|\left(\sum_{\nu\in\Xi_h\cap\partial\mathsf{P}} |v_h(\nu)|^2 + \left|\frac{1}{|\mathsf{P}|}\int_\mathsf{P} v_h\,\mathrm{d}V\right|^2\right) \qquad \forall v_h \in \widehat{V}_h. \tag{4.15}$$

This inequality can be proved by the using the same argument of the proof of Lemma 4.5. Essentially, once the values of degrees of freedom of $v_h \in \widehat{V}_h$ are fixed, we must show that both left and right hand sides in (4.15) vary continuously with respect to $X \in \Sigma$, *i.e.*, on the corresponding set of polygons $\mathsf{P}(X)$. Such property is obvious for the right-hand side in (4.15) since this latter can be directly expressed in terms of the degrees of freedom of v_h, *i.e.*, pointwise values at vertices and average on P. For the left-hand side, we argument as follows in accordance with the proof of Lemma 4.5. Given any sequence of polygonal cells $\mathsf{P}_k = \mathsf{P}_k(X_k)$ convergent to P for $k \to +\infty$, we build the functions $v_h^k \in \widehat{V}_{h|_\mathsf{P}}$ as in the proof of Lemma 4.5. Then, using again the maps ϕ^k, $k \in \mathbb{N}$, we obtain that $\|v_h^k\|_{L^2(\mathsf{P}_k)} \to \|v_h\|_{L^2(\mathsf{P})}$ as $k \to +\infty$. □

We can now show the proof of Theorem 4.1. Let the error $e = u - u_h$. First using the stability property (3.8) and the coercivity of $\mathcal{A}(\cdot,\cdot)$, then by simple manipulations, we obtain

$$\widetilde{\alpha}\,|u-u_h|^2_{H^1\Omega} \le \mathcal{A}\big(u-u_h, e\big) = T_r + T_l + T_c, \tag{4.16}$$

where $\widetilde{\alpha}$ is a strictly positive constant and

$$\begin{aligned}T_r &= \mathcal{A}\big(u-u_h, e-e_\mathfrak{C}\big),\\ T_l &= \mathcal{A}\big(u, e_\mathfrak{C}\big) - \mathcal{A}_h\big(u_h, e_\mathfrak{C}\big),\\ T_c &= \mathcal{A}_h\big(u_h, e_\mathfrak{C}\big) - \mathcal{A}\big(u_h, e_\mathfrak{C}\big).\end{aligned}$$

We first bound the term T_r. We apply equation (2.3), integrate by parts on the *whole* domain Ω recalling that $u_h \in H^2(\Omega) \cap H_0^1(\Omega)$, use the Cauchy–Schwarz inequality and Lemma 4.6 to obtain

$$\begin{aligned} T_r &= (f, e - e_{\mathfrak{C}}) + (\Delta u_h, e - e_{\mathfrak{C}}) \\ &\leq \sum_{\mathsf{P}\in\Omega_h} \|f + \Delta u_h\|_{L^2(\mathsf{P})} \|e - e_{\mathfrak{C}}\|_{L^2(\mathsf{P})} \\ &\leq C \sum_{\mathsf{P}\in\Omega_h} h_{\mathsf{P}} \|f + \Delta u_h\|_{L^2(\mathsf{P})} |e|_{H^1(\omega_{\mathsf{P}})} \\ &\leq C \left(\sum_{\mathsf{P}\in\Omega_h} h_{\mathsf{P}}^2 \|f + \Delta u_h\|_{L^2(\mathsf{P})}^2 \right)^{1/2} |e|_{H^1(\Omega)}. \end{aligned} \tag{4.17}$$

Note that in the last bound above we used the fact that, thanks to Assumption 1, it is easy to check that every polygon P has a uniformly bounded number of neighbors. By definition of L^2 projection, $\pi_m^{\mathsf{P}} \Delta u_h$ minimizes the L^2 distance from Δu_hin the space $\mathbb{P}_m(\mathsf{P})$. Therefore, since $\Delta \Pi_m^{\mathsf{P}} u_h \in \mathbb{P}_{m-2}(\mathsf{P}) \subset \mathbb{P}_m(\mathsf{P})$, it holds

$$h_{\mathsf{P}} \|\Delta u_h - \pi_m^{\mathsf{P}} \Delta u_h\|_{L^2(\mathsf{P})} \leq h_{\mathsf{P}} \|\Delta u_h - \Delta \Pi_m^{\mathsf{P}} u_h\|_{L^2(\mathsf{P})}. \tag{4.18}$$

In view of inequality (4.18), the inverse estimate in Lemma 4.5, the coercivity of $\mathcal{A}_{\mathsf{P}}$ and the stability property (3.8), it holds that

$$\begin{aligned} h_{\mathsf{P}} \|\Delta u_h - \pi_m^{\mathsf{P}} \Delta u_h\|_{L^2(\mathsf{P})} &\leq h_{\mathsf{P}} |u_h - \Pi_m^{\mathsf{P}} u_h|_{H^2(\mathsf{P})} \leq C |u_h - \Pi_m^{\mathsf{P}} u_h|_{H^1(\mathsf{P})} \\ &\leq C \mathcal{A}_{\mathsf{P}} \left(u_h - \Pi_m^{\mathsf{P}} u_h, u_h - \Pi_m^{\mathsf{P}} u_h\right)^{1/2} \leq C\, \eta_{\mathsf{P}}^c. \end{aligned} \tag{4.19}$$

Combining (4.17) with (4.19) it easily follows

$$T_r \leq C \left(\sum_{\mathsf{P}\in\Omega_h} h_{\mathsf{P}}^2 \left(\|f + \pi_m^{\mathsf{P}} \Delta u_h\|_{L^2(\mathsf{P})}^2 + (\eta_{\mathsf{P}}^c)^2 \right) \right)^{1/2} |e|_{H^1(\Omega)} \tag{4.20}$$

$$= C \left(\sum_{\mathsf{P}\in\Omega_h} (\eta_{\mathsf{P}}^r)^2 + (\eta_{\mathsf{P}}^c)^2 \right)^{1/2} |e|_{H^1(\Omega)}. \tag{4.21}$$

In order to bound T_l, we observe that (2.3) and (3.1) imply that

$$T_l = (f, e_{\mathfrak{C}}) - (f_h, e_{\mathfrak{C}}).$$

Now, let $\overline{e}_{\mathfrak{C}}$ be the piecewise constant function given, on each element P, by the average of $e_{\mathfrak{C}}$ on P. Since on each element $f_h = \pi_{m-2}^{\mathsf{P}}(f)$, $m \geq 2$, it holds that

$$T_l = (f - f_h, e_{\mathfrak{C}} - \overline{e}_{\mathfrak{C}}) \leq \sum_{\mathsf{P}\in\Omega_h} \|f - f_h\|_{L^2(\mathsf{P})} \|e_{\mathfrak{C}} - \overline{e}_{\mathfrak{C}}\|_{L^2(\mathsf{P})}. \tag{4.22}$$

We apply a standard error estimate, we use the result of Lemma 4.6 and the definition of η_{P}^l in (4.5), and, then, we apply the Cauchy–Schwarz inequality. Inequality (4.22) becomes

$$T_l \leq C \sum_{\mathsf{P}\in\Omega_h} \eta_{\mathsf{P}}^l \, |e_{\mathfrak{C}}|_{H^1(\mathsf{P})} \leq C \left(\sum_{\mathsf{P}\in\Omega_h} (\eta_{\mathsf{P}}^l)^2 \right)^{1/2} |e|_{H^1(\Omega)}. \tag{4.23}$$

To bound the last term, we add and subtract $\Pi^{\mathsf{P}}_m u_h$ in the arguments of T_c, we use the consistency property (3.7) and we apply the Cauchy–Schwarz inequality on the bilinear forms $\mathcal{A}_h$ and $\mathcal{A}$. We obtain:

$$\begin{aligned} T_c &= \mathcal{A}_h\big(u_h - \Pi^{\mathsf{P}}_m u_h, e_{\mathfrak{C}}\big) - \mathcal{A}\big(u_h - \Pi^{\mathsf{P}}_m u_h, e_{\mathfrak{C}}\big) \\ &\le \mathcal{A}_h\big(u_h - \Pi^{\mathsf{P}}_m u_h, u_h - \Pi^{\mathsf{P}}_m u_h\big)^{1/2} \mathcal{A}_h\big(e_{\mathfrak{C}}, e_{\mathfrak{C}}\big)^{1/2} \\ &\quad + \mathcal{A}\big(u_h - \Pi^{\mathsf{P}}_m u_h, u_h - \Pi^{\mathsf{P}}_m u_h\big)^{1/2} \mathcal{A}\big(e_{\mathfrak{C}}, e_{\mathfrak{C}}\big)^{1/2}. \end{aligned} \tag{4.24}$$

Then, in (4.24) we use the stability property (3.8), the H^1 continuity of $\mathcal{A}$, and the results of Lemma 4.6 and we obtain the final inequality

$$\begin{aligned} T_c &\le C\mathcal{A}_h\big(u_h - \Pi^{\mathsf{P}}_m u_h, u_h - \Pi^{\mathsf{P}}_m u_h\big)^{1/2} |e_{\mathfrak{C}}|_{H^1(\Omega)} \\ &\le C \left(\sum_{\mathsf{P}\in\Omega_h} (\eta^c_{\mathsf{P}})^2 \right)^{1/2} |e|_{H^1(\Omega)}. \end{aligned} \tag{4.25}$$

Finally, the assertion of Theorem 4.1 follows by combining equation (4.16) with inequalities (4.20), (4.23) and (4.25).

We end this section with the following corollary, which states that the error estimator η is also a bound from above of the approximation error.

Corollary 4.7. *Under the same mesh assumptions of Theorem 4.1 it holds*

$$\|u - u_h\|^2_{H^1(\Omega)} + \sum_{\mathsf{P}\in\Omega_h} |u - \Pi^{\mathsf{P}}_m u|^2_{H^1(\mathsf{P})} \le C\eta^2$$

with C independent of h.

Proof. From the stability property in (3.8) and the coercivity/continuity properties in H^1 of $\mathcal{A}_{\mathsf{P}}$ it follows that

$$\eta^c_{\mathsf{P}} \simeq |u_h - \Pi^{\mathsf{P}}_m u_h|_{H^1(\mathsf{P})}, \tag{4.26}$$

where the equivalence holds up to mesh independent constants. Therefore, by using the triangle inequality, the bound in (4.26) and the H^1 continuity of the projection Π^{P}_m we have

$$\begin{aligned} |u - \Pi^{\mathsf{P}}_m u|_{H^1(\mathsf{P})} &\le |u - u_h|_{H^1(\mathsf{P})} + |u_h - \Pi^{\mathsf{P}}_m u_h|_{H^1(\mathsf{P})} + |\Pi^{\mathsf{P}}_m u_h - \Pi^{\mathsf{P}}_m u|_{H^1(\mathsf{P})} \\ &\le C\left(|u - u_h|_{H^1(\mathsf{P})} + \eta^c_{\mathsf{P}}\right). \end{aligned}$$

The assertion of the corollary follows from summing over all the elements and applying Theorem 4.1. □

4.3. Efficiency of the error estimator

In the present section we discuss the efficiency of our error estimator. For simplicity, we assume that the loading term f is a piecewise polynomial of a fixed degree. This is a rather standard assumption in deriving the efficiency of error estimators, that allows to neglect oscillation effects (see for instance [17, 25]).

Theorem 4.8. *Let f be a piecewise polynomial of a fixed degree. Under the same assumptions of Theorem 4.1 and the assumption above on f, it holds*

$$(\eta^r_{\mathsf{P}})^2 + (\eta^c_{\mathsf{P}})^2 + (\eta^l_{\mathsf{P}})^2 \le C\left(|u - u_h|^2_{H^1(\mathsf{P})} + |u - \Pi^{\mathsf{P}}_m u|^2_{H^1(\mathsf{P})}\right) \quad \forall \mathsf{P} \in \Omega_h,$$

with C independent of P.

Proof. We show this proof briefly. The consistency term η^c_{P} can be bounded through (4.26) and the triangle inequality

$$\eta^c_{\mathsf{P}} \leq |u_h - u|_{H^1(\mathsf{P})} + |u - \Pi^{\mathsf{P}}_m u|_{H^1(\mathsf{P})} + |\Pi^{\mathsf{P}}_m u - \Pi^{\mathsf{P}}_m u_h|_{H^1(\mathsf{P})},$$

and, then, by recalling the H^1 continuity of the projection operator Π^{P}_m.

To derive an upper bound for the residual term η^r_{P}, we first add and subtract $\Delta u_{h,\mathsf{P}}$, and, then, we apply the triangle inequality to obtain

$$\eta^r_{\mathsf{P}} \leq h_{\mathsf{P}} \|f + \Delta u_{h,\mathsf{P}}\|_{L^2(\mathsf{P})} + h_{\mathsf{P}} \|(\mathcal{I} - \pi^{\mathsf{P}}_m)\Delta u_{h,\mathsf{P}}\|_{L^2(\mathsf{P})} \tag{4.27}$$

where $\mathcal{I}$ denotes the identity operator. As f is polynomial on each element by hypothesis, the first term in the right-hand side of inequality(4.27) can be bounded using standard techniques of the finite element analysis (see for instance [38])

$$h_{\mathsf{P}} \|f + \Delta u_{h,\mathsf{P}}\|_{L^2(\mathsf{P})} \leq C|u - u_h|_{H^1(\mathsf{P})}.$$

For the second term in (4.27), we make use of the same argument as in the derivation of (4.19). More precisely, from the definition of π^{P}_m and the fact that $\Delta \Pi^{\mathsf{P}}_m u_h \in \mathbb{P}_{m-2}(\mathsf{P})$ it follows that

$$\|(\mathcal{I} - \pi^{\mathsf{P}}_m)\Delta u_{h,\mathsf{P}}\|_{L^2(\mathsf{P})} = \|(\mathcal{I} - \pi^{\mathsf{P}}_m)\Delta(u_{h,\mathsf{P}} - \Pi^{\mathsf{P}}_m u_h)\|_{L^2(\mathsf{P})}.$$

The above bound, the L^2 continuity of π^{P}_m and the inverse estimate (4.5) yield the inequality

$$h_{\mathsf{P}} \|(\mathcal{I} - \pi^{\mathsf{P}}_m)\Delta u_{h,\mathsf{P}}\|_{L^2(\mathsf{P})} \leq C|u_{h,\mathsf{P}} - \Pi^{\mathsf{P}}_m u_h|_{H^1(\mathsf{P})}. \tag{4.28}$$

Finally, the bound for the second term in (4.27) follows from (4.28), (4.26) and from recalling that the term η^c_{P} has already been bounded.

For the loading term, by using (2.1) and the definition of the discrete load in Section 3.5 we have

$$\eta^l_{\mathsf{P}} = h_{\mathsf{P}} \|\Delta u - \pi^{\mathsf{P}}_{m-2}\Delta u\|_{L^2(\mathsf{P})} = h_{\mathsf{P}} \|(\mathcal{I} - \pi^{\mathsf{P}}_{m-2})\Delta u\|_{L^2(\mathsf{P})}.$$

Then, from arguments and manipulations similar to those used above for the η^r_{P} term, we obtain

$$\eta^l_{\mathsf{P}} \leq h_{\mathsf{P}} \|\Delta(u - \Pi^{\mathsf{P}}_m u)\|_{L^2(\mathsf{P})}. \tag{4.29}$$

Let us now recall that $f = -\Delta u$ is a piecewise polynomial of a given degree on P and the same holds for $\Delta(\Pi^{\mathsf{P}}_m u)$. Therefore, from multiplication by a bubble function and usual techniques in a-posteriori error estimation it follows that (4.29) that

$$\eta^l_{\mathsf{P}} \leq C|u - \Pi^{\mathsf{P}}_m u|_{H^1(\mathsf{P})}$$

with C is a constant factor independent of the element P. □

Remark 4.9. The result above shows that the error estimator is bounded by the error plus an approximation term of the same order, ensuing from the (necessary) projections in the estimator. Note that, as shown in Corollary 4.7, the error estimator η is an upper bound also for such approximation term.

5. Numerical experiments

In this section, we investigate the behavior of the error estimator by solving the boundary value problem (2.3) in two benchmark cases that differ in the shape of the computational domain Ω and in the regularity of the exact solution. We show the performance of the estimator coupled with a simple mesh adaptive strategy by comparing the convergence errors obtained on a sequence of meshes that are either uniformly or adaptively refined starting from a given base mesh. These meshes are formed by different types of cells such as pattern-distorted quadrilaterals and hexagons. The first mesh of each sequence is shown in Figure 2. Other choices of

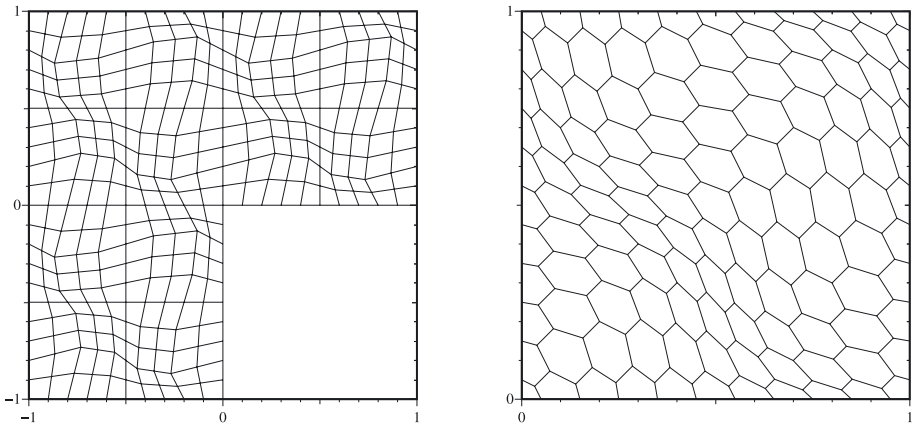

FIGURE 2. The starting mesh of the sequence of adaptive and uniform refinement for test case 1 (left plot) and test case 2 (right plot).

cells were considered in a preliminary stage of this work in agreement with the mesh regularity constraint of Assumption 1 and using these meshes we obtained very similar results.

The uniform refinement process is implemented by generating the refined mesh with a finer mesh size parameter. Specific details are given in the description of each test case. This strategy preserves the conformity and shape regularity of the mesh. Instead, an adaptively refined mesh is generated from a given mesh by refining each element that has been marked for refinement in accordance with the local error estimate provided by our error indicator. To refine a marked element P with z_{P} vertices and edges we subdivide it into z_{P} nested sub-elements by connecting the edge midpoints of each pair of consecutive edges of $\partial\mathsf{P}$ to the center of P. As all the cells of these meshes are convex, we take the barycenter of P as such internal point. All the sub-elements generated by this process are quadrilaterals disregarding the shape of the parent mesh element. Starting from the coarsest base mesh, the adaptively refinement strategy proceeds as follows:

(i) we calculate all the local element error indicators η_{P}, for $\mathsf{P} \in \Omega_h$;

(ii) we sort the elements in accordance with the value of the estimated error;

(iii) we mark the elements for refinement starting from the one with the biggest estimated error until one of the two following conditions is satisfied:
- at least 20% of the elements has been marked;
- the sum of the estimated errors η_{P} of the cells that are marked for refinement is bigger than an assigned fraction (typically 30–50%) of the total estimated error;

(iv) we sub-divide all marked elements as described above.

This strategy preserves the shape regularity of the base mesh but leads in general to non-conforming meshes, which are still acceptable for the VEM. As the VEM can be applied to non-conforming meshes, we avoid the artificial refinement of the unmarked neighboring elements as is required, for example, in the *red-blue-green* strategies for triangular meshes [38]. Note that the theoretical error estimates for the method are valid for mesh families with the uniform bound on the number of edges required by our mesh regularity assumptions. Therefore, we should, in principle, insert an automatic check in order to avoid an uncontrolled growth of the number of hanging nodes. However, in all the tests that we performed, the presence of such a check proved almost worthless as the number of edges per element seemed to stay naturally rather limited.

For each test case, we first present a plot of the convergence errors for the uniform and the adaptive refinement, followed by a plot for the three different terms

$$\eta^* = \left(\sum_{\mathsf{P}\in\Omega_h} (\eta_{\mathsf{P}}^*)^2 \right)^{1/2} \quad \text{with} \quad * = r, l, c$$

where η_{P}^r, η_{P}^l, and η_{P}^c are defined in (4.4), (4.5), (4.6), respectively. We also show a picture of the adaptively refined mesh for each adaptive calculation at an intermediate refinement step. Finally, we present a comparison (ratio) between the estimated error η and the error $\|u-u_h\|_{1,h}$, evaluated in a discrete H^1-type norm described below. Although such quantity is not a true efficienty index (the reason being that we are not using exactly the H^1 norm in evaluating the error), the ratio above still gives valuable information on the estimator's behaviour.

Since the discrete solution u_h is unknown inside the element, we evaluate the H^1-norm of the error through the following mesh-dependent norm:

$$\|v_h\|_{1,h}^2 = \sum_{\mathsf{P}\in\Omega_h} \|v_h\|_{1,h,\mathsf{P}}^2, \tag{5.1}$$

where each term $\|v_h\|_{1,h,\mathsf{P}}^2$ is a local approximation of the square of the energy seminorm of v_h. For $m \geq 2$, this local contribution reads as:

$$\begin{aligned}\|v_h\|_{1,h,\mathsf{P}}^2 = &\sum_{\mathsf{e}\in\partial\mathsf{P}} h_{\mathsf{P}} \, |v_h|_{H^1(\mathsf{e})}^2 + \sum_{\mathsf{e}\in\partial\mathsf{P}} h_{\mathsf{P}} \|\partial_n v_h\|_{L^2(\mathsf{e})}^2 \\ &+ \left(\frac{1}{|\mathsf{P}|} \int_{\mathsf{P}} v_h \, \mathrm{d}V - \overline{v}_{h,\mathsf{P}} \right)^2 + \sum_{j=1}^{m-2} \sum_{q\in\mathcal{M}_j(\mathsf{P})} \left(\frac{1}{|\mathsf{P}|} \int_{\mathsf{P}} v_h q \, \mathrm{d}V \right)^2,\end{aligned} \tag{5.2}$$

where $\overline{v}_{h,\mathsf{P}}$ is the arithmetic mean of the values that v_h takes at the $N_{\mathsf{P}}^{\mathcal{V}_h}$ vertices of the element P (here denoted by v_{v}), *i.e.*,

$$\overline{v}_{h,\mathsf{P}} = \frac{1}{N_{\mathsf{P}}^{\mathcal{V}_h}} \sum_{\mathsf{v}\in\partial\mathsf{P}} v_{\mathsf{v}}. \tag{5.3}$$

It is easy to check that the kernel of seminorm (5.2) is given by the constant functions, and that this seminorm scales like the H^1-seminorm. Therefore, norm $\|\cdot\|_{1,h}$ represents an H^1-type discrete norm. Recalling Theorem 3.7, we therefore expect that, under the same hypotheses, the rate of convergence measured by norm (5.1) will satisfy

$$\|u_h - u\|_{1,h,\mathsf{P}} \leq C h^m \, |u|_{H^{m+1}(\Omega)},$$

as it holds for the H^1-norm.

5.1. Test Case 1: the L-shaped domain

Let us consider the boundary value problem (2.3) on the L-shaped domain obtained by carving out the lower right quarter from the square domain $[-1,1]^2$. The source term f is zero everywhere, and the boundary conditions are set in accordance with the exact solution

$$u(r,\theta) = r^{2/3} \sin(2\theta/3),$$

which is here expressed in terms of the polar coordinates (r,θ) in the plane. The initial grid adopted in this test is given by applying a coordinate transformation mapping

$$\begin{aligned} x &= \xi + \phi \sin(2\pi\xi) \sin(2\pi\zeta), \\ y &= \zeta + \phi \sin(2\pi\xi) \sin(2\pi\zeta), \end{aligned}$$

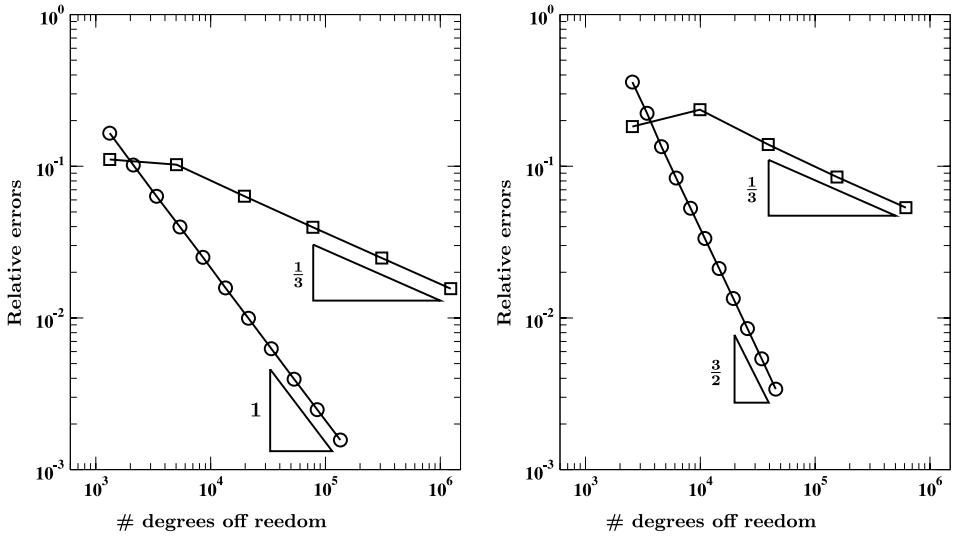

FIGURE 3. Test 1. Solution with a corner singularity on an L-shaped domain using distorted quadrilateral meshes. Relative error curves for the adaptively refined calculations (circles) and the uniformly refined calculations (squares) for the virtual element schemes using $m = 2$ (left plot) and $m = 3$ (right plot).

with distortion parameter $\phi = 1$ to a regular grid of squares in the coordinates system (ξ, ζ), see, *e.g.*, reference [22] for more details. Although the load is regular, the exact solution u is only in $H^{5/3}(\Omega)$ due to the presence of the re-entrant corner. Thus, the expected asymptotic rate of convergence on the sequence of the uniformly refined meshes is $\mathsf{err} = \mathcal{O}(N^{-1/3})$, where N is the total number of degrees of freedom, since on such meshes the scaling $N = \mathcal{O}(h^{-2})$ approximately holds. Conversely, a successful adaptive strategy should recover the optimal convergence rate of regular problems, which is $\mathsf{err} = \mathcal{O}(N^{-m/2})$. Therefore, we expect $\mathsf{err} = \mathcal{O}(N^{-1})$ for quadratic polynomials and $\mathsf{err} = \mathcal{O}(N^{-3/2})$ for cubic polynomials.

We illustrate the numerical results Figures 3–5 and the refined meshes in Figure 6. The plots on the left refer to the calculations for $m = 2$, the plots on the right to the calculations for $m = 3$. The good behavior of the adaptive strategy combined with the *a-posteriori* estimator is reflected by the slopes of the error curves of the two plots in Figure 3. These errors are marked by circles when the meshes are adaptively refined and by squares when the meshes are uniformly refined. The slopes of the error curves are close to -1 for $m = 2$ and $-3/2$ for $m = 3$ for the adaptive calculations, while they are close to $-1/3$ when the meshes are uniformly refined in agreement with the regularity of the solution. The plots in Figure 4 show the behavior of the different terms forming the error estimator in Theorem 4.1, *i.e.*, η^r (circles) and η^c (squares). Since the load term of this problem is zero, the third term η^l is always zero and is not displayed. As expected from theoretical consideration, these two terms properly scale like $\mathcal{O}(N^{-m/2})$. The two plots in Figure 5 show the good (robust in h) behavior of the ratio among η and the discrete H^1-type norm of the error $\|u - u_h\|_{1,h}$. The two plots in Figure 6 show how the adaptive strategy correctly refines near the re-entrant corner.

5.2. Test Case 2: load with strong internal layer

In this test case, we consider the boundary value problem (2.3) defined on the square domain $\Omega =]0, 1[^2$ by choosing the boundary conditions and the load term consistent with the exact solution:

$$u(x, y) = 16x(1 - x)y(1 - y)\arctan(25x - 100y + 50), \qquad (x, y) \in \Omega.$$

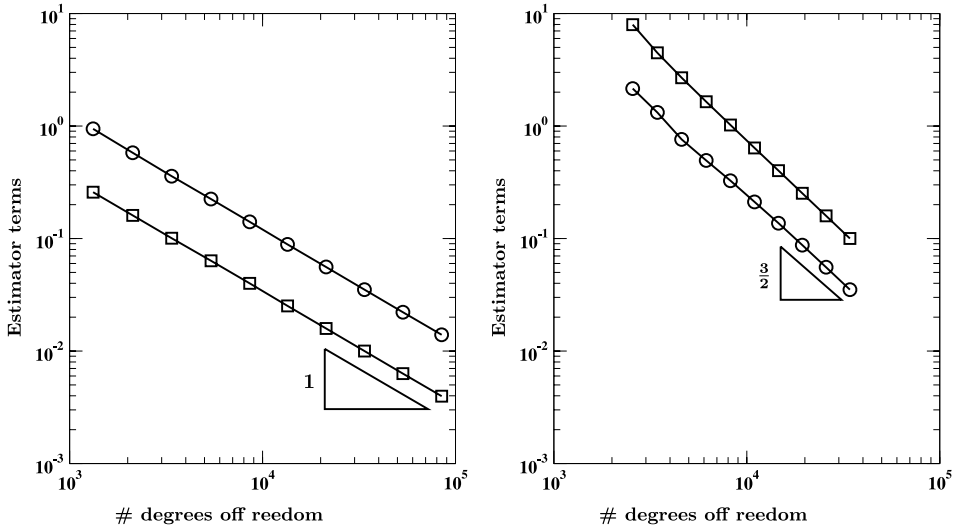

FIGURE 4. Test 2. Solution with a corner singularity on an L-shaped domain using distorted quadrilateral meshes. Estimator terms η^r (circles) and η^c (squares) for the virtual element schemes using $m = 2$ (left plot) and $m = 3$ (right plot).

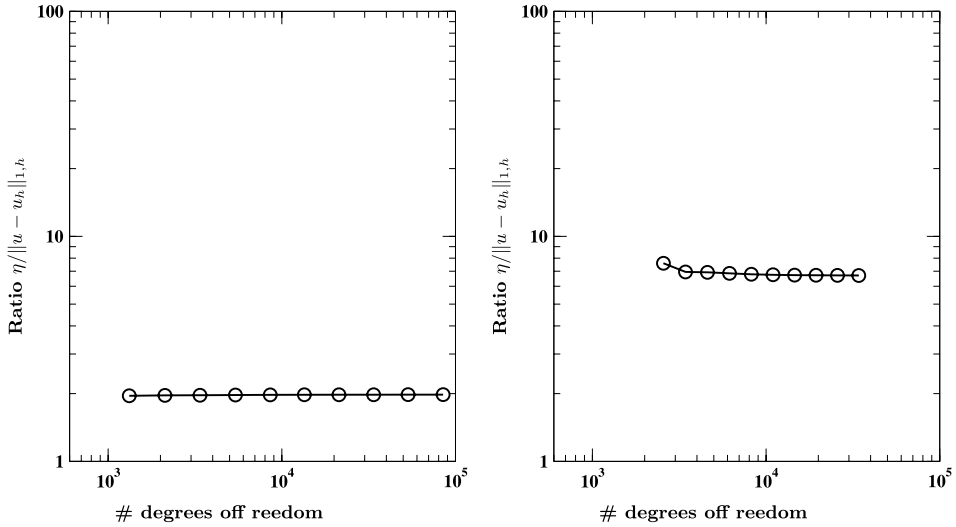

FIGURE 5. Test 2. Solution with a corner singularity on an L-shaped domain using distorted quadrilateral meshes. Ratio among η and $\|u - u_h\|_{1,h}$ for the virtual element schemes using $m = 2$ (left plot) and $m = 3$ (right plot).

The starting mesh for both uniformly and adaptively refined calculations is mainly formed by hexagons built by a dualization procedure from a uniform triangle-based mesh.

As the exact solution u belongs to $H^2(\Omega)$ and the domain Ω is regular, the asymptotic convergence rate of the numerical approximation on uniformly and adaptively refined meshes is expected to be $\mathsf{err} = \mathcal{O}(N^{-1/2})$, where N is the total number of degrees of freedom, because of the approximate scaling $N = \mathcal{O}(h^{-2})$. Nonetheless, the exact solution u is characterized by a region with a very strong gradient around the line of equation $y = 1/2+x/4$

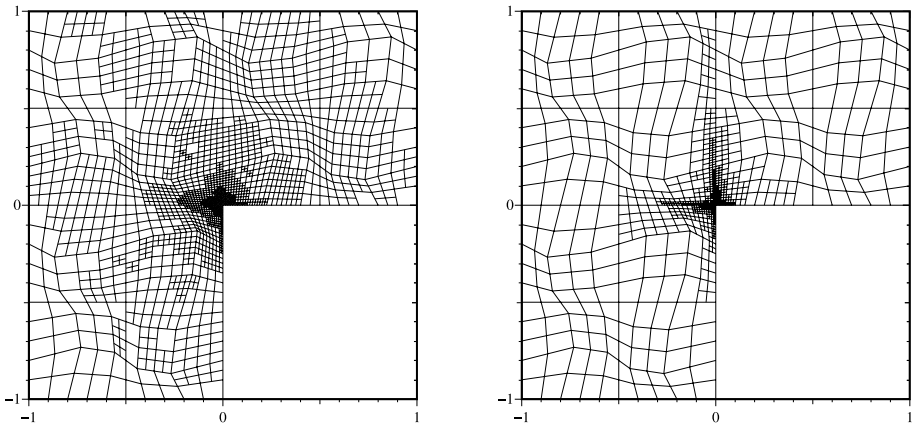

FIGURE 6. Test 1. The mesh after four adaptive refinements for the virtual element schemes using $m = 2$ (left plot) and $m = 3$ (right plot).

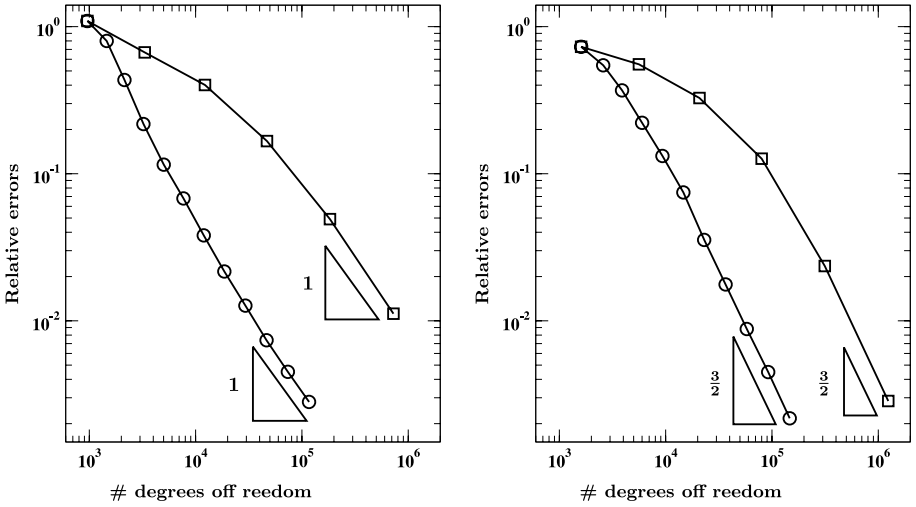

FIGURE 7. Test 2. Strong internal layer solution on a square domain using mainly hexagonal meshes. Relative error curves for the adaptively refined calculations (circles) and the uniformly refined calculations (squares) for the virtual element schemes using $m = 2$ (left plot) and $m = 3$ (right plot).

and the numerical approximation to u will attain the theoretical convergence rate only after that this internal layer has been resolved. To resolve this internal layer requires that the size of the elements in this strong gradient region become sufficiently small. When the mesh is uniformly refined such meshes are characterized by a very large number of mesh elements N and the VEM requires a huge number of degrees of freedom. Conversely, we expect the solutions obtained with the adaptive strategy to follow the theoretical rate in N also for rather inexpensive grids.

We illustrate the numerical results in Figures 7–9 and the refined meshes in Figure 10. As for the previous test case, the plots on the left refer to the calculations for $m = 2$, the plots on the right to the calculations for $m = 3$. The two plots in Figure 7 shows the curves for the approximation errors given by the adaptive strategy driven by the a-posteriori estimator (circles) and when the uniform refinement is adopted (squares).

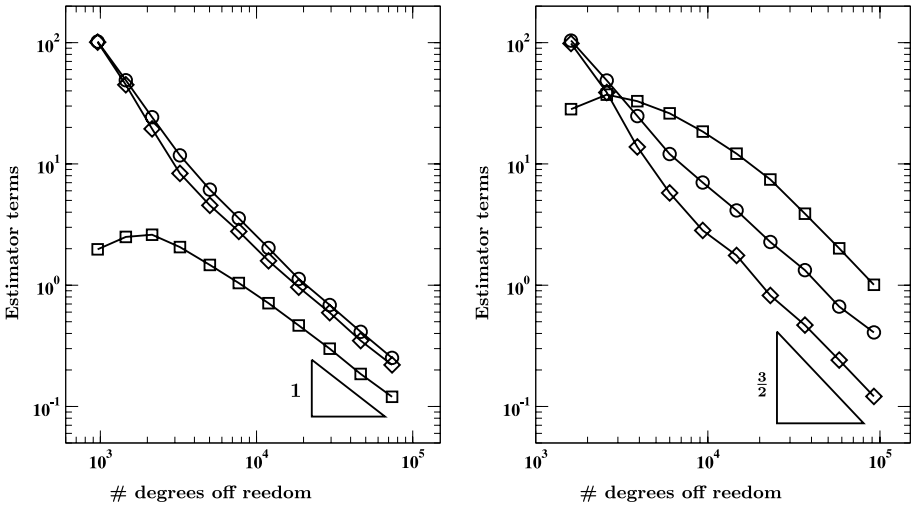

FIGURE 8. Test 2. Strong internal layer solution on a square domain using mainly hexagonal meshes. Estimator terms η^r (circles), η^l (squares) and η^c (diamonds) for the scheme with $m = 2$ (left plot) and $m = 3$ (right plot).

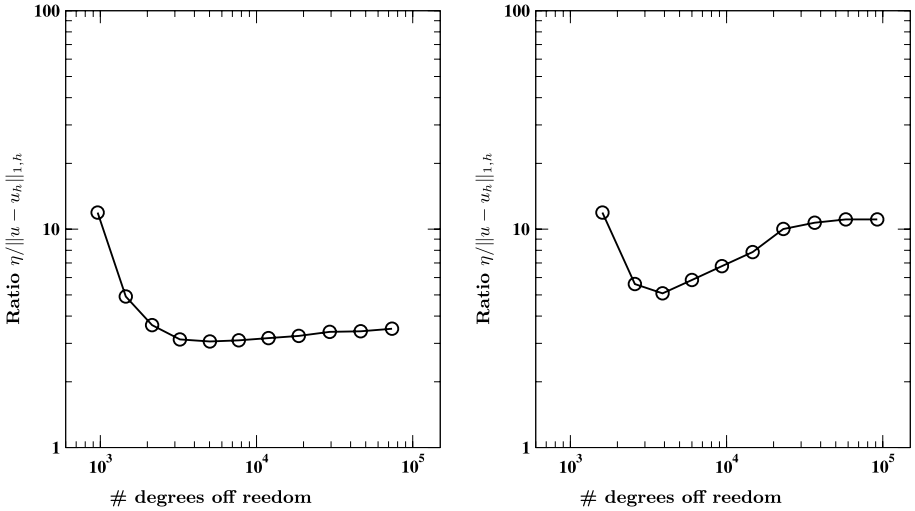

FIGURE 9. Test 2. Strong internal layer solution on a square domain using mainly hexagonal meshes. Ratio among η and $\|u-u_h\|_{1,h}$ for the scheme with $m = 2$ (left plot) and $m = 3$ (right plot).

In both cases, the slopes of the error curves are asymptotically close to -1 for $m = 2$ and $3/2$ for $m = 3$ for the adaptive calculations. However, the adaptive strategy requires about one tenth of the degrees of freedom of the uniformly refined strategy to provide a numerical solution with about the same level of accuracy. The plots in Figure 8 show the behavior of the different terms forming the error estimator in (4.4), (4.5), and (4.6), *i.e.*, η^r (circles), η^l (squares), and η^c (diamonds). As expected from theoretical consideration, these two terms properly scale like $\mathcal{O}(N^{-m/2})$. The two plots in Figure 9 show the good (robust in h) behavior of the ratio among η and the discrete H^1-type norm of the error $\|u-u_h\|_{1,h}$. Note moreover that the value of such ratio is,

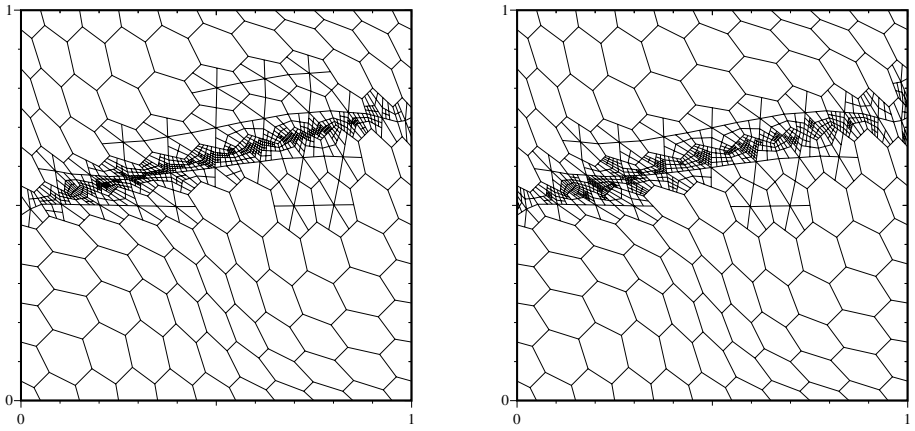

FIGURE 10. Test 2. The mesh after four adaptive refinements for the scheme with $m = 2$ (left plot) and $m = 3$ (right plot).

for Test cases 1,2 (and fixed $m = 2$ or 3), always around the same value. This seems to indicate a robustness of the error indicator also with respect to the problem and not only with respect to the mesh. Such observation suggests that a rather accurate indication of the global error could be computed by scaling the estimator by a fixed factor depending on m. A thorough numerical investigation would be required to assess this point. Finally, the two plots in Figure 10 show how the adaptive strategy correctly refines in a neighborhood of the internal layer.

6. Conclusions

A residual based *a posteriori* error estimator for the virtual element method introduced in reference [9] was proposed. Indeed, the mesh flexibility of the virtual element method makes it a very appealing ground for the application of mesh adaptation strategies. The challenge in this work is that the lack of knowledge of the basis functions makes the development and theoretical analysis of error estimators rather involved. The reliability and efficiency of the estimator was theoretically proved and its performance in combination with an adaptive strategy was investigated numerically.

Acknowledgements. The work of the second author was supported by the Laboratory Directed Research and Development (LDRD) Program (project LDRD 20140270ER) and the DOE Office of Science Advanced Scientific Computing Research (ASCR) Program in Applied Mathematics under the auspices of the National Security Administration of the U.S. Department of Energy by Los Alamos National Laboratory, operated by Los Alamos National Security LCC under contract DE-AC52-06NA25396.

References

[1] B. Ahmed, A. Alsaedi, F. Brezzi, L.D. Marini and A. Russo, Equivalent projectors for virtual element methods. *Comput. Math. Appl.* **66** (2013) 376–391.

[2] M. Ainsworth and J.T. Oden, *A posteriori* error estimation in finite element analysis. *Comput. Methods Appl. Mech. Eng.* **142** (1997) 1–88.

[3] P.F. Antonietti, L. Beirão da Veiga, C. Lovadina and M. Verani, Hierarchical *a posteriori* error estimators for the mimetic discretization of elliptic problems. *SIAM J. Numer. Anal.* **51** (2013) 654–675.

[4] I. Babuska and W.C. Rheinboldt, Error estimates for adaptive finite element computations. *SIAM J. Numer. Anal.* **15** (1978) 736–754.

[5] R.E. Bank and E. Weiser, Some *a posteriori* error estimators for elliptic partial differential equations. *Math. Comput.* **44** (1985) 283–301.

[6] L. Beirão da Veiga, A residual based error estimator for the mimetic finite difference method. *Numer. Math.* **108** (2008) 387–406.
[7] L. Beirão da Veiga and K. Lipnikov, A mimetic discretization of the Stokes problem with selected edge bubbles. *SIAM J. Sci. Comput.* **32** (2010) 875–893.
[8] L. Beirão da Veiga and G. Manzini, An *a posteriori* error estimator for the mimetic finite difference approximation of elliptic problems. *Int. J. Numer. Meth. Eng.* **76** (2008) 1696–1723.
[9] L. Beirão da Veiga and G. Manzini, A virtual element method with arbitrary regularity. *IMA J. Numer. Anal.* **34** (2014) 759–781.
[10] L. Beirão da Veiga, K. Lipnikov and G. Manzini, Arbitrary-order nodal mimetic discretizations of elliptic problems on polygonal meshes. *SIAM J. Numer. Anal.* **49** (2011) 1737–1760.
[11] L. Beirão da Veiga, F. Brezzi, A. Cangiani, G. Manzini, L.D. Marini and A. Russo, Basic principles of virtual element methods. *Math. Models Methods Appl. Sci.* **23** (2013) 119–214.
[12] L. Beirão da Veiga, F. Brezzi and L.D. Marini, Virtual Elements for linear elasticity problems. *SIAM J. Num. Anal.* **51** (2013) 794–812.
[13] L. Beirão da Veiga, K. Lipnikov and G. Manzini, The Mimetic Finite Difference Method. In vol. 11 of *Model. Simul. Appl.*, 1st edition. Springer-Verlag, New York (2013).
[14] L. Beirão da Veiga, F. Brezzi, L.D. Marini and A. Russo, The Hitchhiker's Guide to the Virtual Element Method. *Math. Models Methods Appl. Sci.* **24** (2014) 1541–1573.
[15] J.E. Bishop, A displacement-based finite element formulation for general polyhedra using harmonic shape functions. *Int. J. Numer. Methods Eng.* **97** (2014) 1–31.
[16] J. Bonelle and A. Ern, Analysis of compatible discrete operator schemes for elliptic problems on polyhedral meshes. *ESAIM: M2AN* **48** (2014) 553–581.
[17] D. Braess, Finite elements. Theory, fast solvers, and applications in elasticity theory, 3rd edition. Cambridge University Press (2007).
[18] F. Brezzi, A. Buffa and K. Lipnikov, Mimetic finite differences for elliptic problems. *ESAIM: M2AN* **43** (2009) 277–295.
[19] F. Brezzi and L.D. Marini, Virtual element method for plate bending problems. *Comput. Methods Appl. Mech. Eng.* **253** (2013) 455–462.
[20] F. Brezzi, K. Lipnikov and M. Shashkov, Convergence of the mimetic finite difference method for diffusion problems on polyhedral meshes. *SIAM J. Numer. Anal.* **43** (2005) 1872–1896.
[21] S. Brenner and L. Scott, The Mathematical Theory of Finite Element Methods. Springer-Verlag, Berlin/Heidelberg (1994).
[22] A. Cangiani and G. Manzini, Flux reconstruction and pressure post-processing in mimetic finite difference methods. *Comput. Methods Appl. Mech. Eng.* **197** (2008) 933–945.
[23] A. Cangiani, G. Manzini and A. Russo, Convergence analysis of the mimetic finite difference method for elliptic problems. *SIAM J. Numer. Anal.* **47** (2009) 2612–2637.
[24] P.G. Ciarlet, The finite element method for elliptic problems. North-Holland, Amsterdam (1978).
[25] W. Dorfler and R.H. Nochetto, Small data oscillation implies the saturation assumption. *Numer. Math.* **91** (2002) 1–12.
[26] J. Droniou, R. Eymard, T. Gallouët and R. Herbin, A unified approach to mimetic finite difference, hybrid finite volume and mixed finite volume methods. *Math. Models Methods Appl. Sci.* **20** (2010) 265–295.
[27] P. Grisvard, Elliptic problems in nonsmooth domains. In vol. 24 of *Monogr. Stud. Math.* Pitman, Boston (1985).
[28] K. Lipnikov, G. Manzini and D. Svyatskiy, Analysis of the monotonicity conditions in the mimetic finite difference method for elliptic problems. *J. Comput. Phys.* **230** (2011) 2620–2642.
[29] S. Mousavi and N. Sukumar, Numerical integration of polynomials and discontinuous functions on irregular convex polygons and polyhedrons. *Comput. Mech.* **47** (2011) 535–554.
[30] P. Neittaanmki and S. Repin, Error control and a posteriori estimates. Reliable methods for computer simulation. In vol. 33 of *Stud. Math. Appl.* Elsevier Science (2004).
[31] S. Repin, A posteriori Estimates for Partial Differential Equations. In vol. 4 of *Radon Series on Computational and Applied Mathematics*. De Gruyter, Berlin (2008).
[32] R. Stenberg, A technique for analysing finite-element methods for viscous incompressible flow. *Int. J. Numer. Meth. Fluids* **11** (1990) 935–948.
[33] N. Sukumar and E. Malsch, Recent advances in the construction of polygonal finite element interpolants. *Arch. Comput. Methods Eng.* **13** (2006) 129–163.
[34] N. Sukumar and A. Tabarraei, Conforming polygonal finite elements. *Int. J. Numer. Meth. Eng.* **61** (2004) 2045–2066.
[35] C. Talischi and G.H. Paulino, Addressing integration error for polygonal finite elements through polynomial projections: A patch test connection. *Math. Models Methods Appl. Sci.* **24** (2014) 1701–1727.
[36] C. Talischi, G.H. Paulino, A. Pereira and I.F.M. Menezes, Polygonal finite elements for topology optimization: A unifying paradigm. *Int. J. Numer. Methods Eng.* **82** (2010) 671–698.
[37] C. Talischi, A. Pereira, G.H. Paulino, I.F.M. Menezes and M.S. Carvalho, Polygonal finite elements for incompressible fluid flow. *Int. J. Numer. Methods Fluids* **74** (2014) 134–151.
[38] R. Verfürth, A review of a posteriori error estimation and adaptive mesh refinement. Wiley and Teubner, Stuttgart (1996).
[39] M. Vohralik, Guaranteed and fully robust a posteriori error estimates for conforming discretizations of diffusion problems with discontinuous coefficients. *J. Sci. Comput.* **46** (2011) 397–438.
[40] M. Vohralik and B.I. Wohlmuth, Mixed finite element methods: implementation with one unknown per element, local flux expressions, positivity, polygonal meshes, and relations to other methods. *Math. Model. Methods Appl. Sci.* **23** (2013) 803–838.
[41] E. Wachspress, A rational Finite Element Basis. Academic Press (1975).